The Astronomical Journal, 151:116 (9pp), 2016 May doi:10.3847/0004-6256/151/5/116

A METHOD TO CALIBRATE THE HIGH-RESOLUTION CATANIA ASTROPHYSICAL OBSERVATORY SPECTROPOLARIMETER

F. Leone[1,2], G. Avila[3], G. Bellassai[2], P. Bruno[2], S. Catalano[2], R. Di Benedetto[2], A. Di Stefano[2], M. Gangi[1,2], M. Giarrusso[1,2], V. Greco[2], E. Martinetti[2], M. Miraglia[2], M. Munari[2], C. Pontoni[2], C. Scalia[1,2], S. Scuderi[2], and P. Spanó[2]

[1] Università di Catania, Dipartimento di Fisica e Astronomia, Sezione Astrofisica, Via S. Sofia 78, I-95123 Catania, Italy
[2] INAF—Osservatorio Astrofisico di Catania, Via S. Sofia 78, I-95123 Catania, Italy
[3] ESO, Karl-Schwarzschild-Straße 2, D-85748, Garching bei München, Germany
Received 2015 October 17; accepted 2016 February 24; published 2016 April 19

ABSTRACT

The Catania Astrophysical Observatory Spectropolarimeter (CAOS) is a white-pupil cross-dispersed échelle spectrograph with a spectral resolution of up to $R = 55{,}000$ in the 375–1100 nm range in a single exposure, with complete coverage up to 856 nm. CAOS is linked to the 36-inch telescope, at Mount Etna Observatory, with a couple of 100 μm optical fibers and it achieves a signal-to-noise ratio better than 60 for a $V = 10$ mag star in one hour. CAOS is thermally stabilized in temperature within a 0.01 K rms, so that radial velocities are measured with a precision better than 100 m s^{-1} from a single spectral line. Linear and circular spectropolarimetric observations are possible by means of a Savart plate working in series with a half-wave and a quarter-wave retarder plate in the 376–850 nm range. As is usual for high-resolution spectropolarimeters, CAOS is suitable to measure all Stokes parameters across spectral lines and it cannot measure the absolute degree of polarization. Observations of unpolarized standard stars show that instrumental polarization is generally zero at 550 nm and can increase up to 3% at the other wavelengths. Since polarized and unpolarized standard stars are useless, we suggest a method to calibrate a high-resolution spectropolarimeter on the basis of the polarimetric properties of spectral lines formed in the presence of a magnetic field. As applied to CAOS, observations of magnetic chemically peculiar stars of the main sequence show that the cross-talk from linear to circular polarization is smaller than 0.4% and that conversion from circular to linear is less than 2.7%. Strength and wavelength dependences of cross-talk can be entirely ascribed, via numerical simulations, to the incorrect retardance of achromatic wave plates.

Key words: instrumentation: polarimeters – instrumentation: spectrographs – methods: observational – techniques: polarimetric – techniques: spectroscopic

1. INTRODUCTION

In the same way that high-resolution spectropolarimetry has given a deep comprehension of solar magnetism (Trujillo-Bueno et al. 2002), any field of astrophysical research would greatly benefit from this observational technique. Many theoretical predictions are hidden in the polarized spectral line profiles, with a fashionable example given by exoplanets whose atmospheres, by analogy with the Earth (Sterzik et al. 2012), could be unveiled by polarimetric studies, particularly looking at the Raman scattering (Clarke & Naghizadeh-Khouei 2000). The extention of high-resolution spectropolarimetry beyond the Sun has been limited by the weakness, usually a few percent, of the polarized signal and faintness of astronomical sources.

With reference to the circular polarization, Solanki & Stenflo (1986) have already discussed the limits of spectropolarimetry due to the spectral resolution. These authors have pointed out that the area and amplitude of a Stokes V profile across spectral lines strongly decreases with instrumental smearing. Resolution effects are quantified here by numerically computing the Stokes profiles for the Fe I 5250.4 Å line as formed in the solar atmosphere assuming a uniform 0.1 Tesla field, tilted by 45° with respect to the observer's line of sight and aligned with respect to the equatorial reference system. The radiative transfer equation has been solved in the presence of a magnetic field with *Codice per la Sintesi Spettrale nelle Atmosfere Magnetiche* (Stift et al. 2012). Figure 1 shows the computed Stokes Q/I profiles for different instrumental resolutions and signal-to-noise ratios (S/N). It appears that at the typical resolution of solar spectrographs ($R = 500{,}000$) even at a very low signal-to-noise ratio (S/N = 30), the Stokes parameters are correctly recovered. Decreasing the instrumental resolution, the Stokes profile progressively disappears and becomes almost null at $R = 20{,}000$, despite a huge S/N. Figure 1 shows that present spectrographs, working at $R = 115{,}000$ (e.g., HARPS), can measure a few percent polarization, easily achieving the necessary S/N for targets with $V \leqslant 10$, and that the same is possible at $R = 50{,}000$ and S/N ~ 200 with a one meter class telescope for objects brighter than $V \sim 8$.

The facilities available to perform high-resolution spectropolarimetry are very limited in number and all at medium size class telescopes. Full Stokes polarimeter is possible with ESPADONS ($R = 68{,}000$) at the 3.6 m Canadian-France-Hawaii Telescope, NARVAL ($R = 65{,}000$) at the 2 m Bernard Lyot Telescope and HARPS ($R = 115{,}000$) at the ESO 3.6 m telescope. New facilities will be soon available, i.e., PEPSI ($R = 120{,}000$) at Large Binocular Telescope (Strassmeier et al. 2015) and HARPS-North Polarimeter ($R = 115{,}000$) at the Telescopio Nazionale Galileo (Leone et al. 2014). In such a context, where long temporal coverages or large surveys cannot be easily accomplished, we decided to realize a new white-pupil échelle spectrograph for the 36-inch telescope of the *Osservatorio Astrofisico di Catania* basically devoted to spectropolarimetry. Because of the limited size of the telescope, resolution was fixed at $R = 55{,}000$ as a compromise between spectral smearing and observability of faint targets.

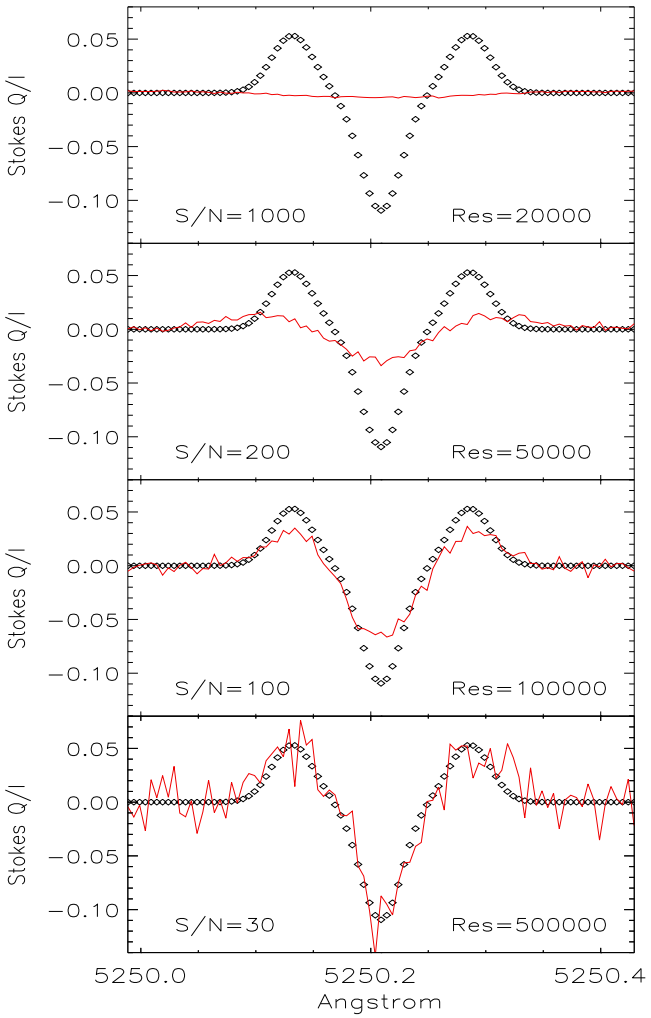

Figure 1. Theoretical (◊'s) Stokes *Q/I* line profile of the Fe I 5018 Å, for a solar spectral region assuming a uniform 0.1 Tesla magnetic field tilted with respect to the observer's line of sight and clockwise rotated with respect to the equatorial reference system of 45°, and their appearance with instrumental smearing and signal-to-noise.

Accuracy in polarimetry is not only a matter of photon statistics (Bagnulo et al. 2013) but it depends on what Serkowski (1974) defined *instrumental polarization*. A kind of *observer effect* due to the interaction of the incoming radiation with the instrumentation that modifies just that polarization status to be measured. Instrumental polarization, for photopolarimeters and low-resolution spectropolarimeters, is usually determined by observing unpolarized and polarized standard stars (Covino et al. 2014) or, more recently, observing the Earth sky (Harrington et al. 2011). Unfortunately, high-resolution spectropolarimeters cannot measure the absolute fluxes with the necessary accuracy to be calibrated by observing standard stars and new methods are required for their calibration.

In the next sections, the *Catania Astrophysical Observatory Spectropolarimeter* (here after CAOS) is described with reference to commissioning results. We also present a method to determine the instrumental polarization of a high-resolution spectrograph based on the full Stokes polarimetry of magnetic stars. We show how the variety of polarimetric properties presented by spectral lines formed in a magnetic field can be used to calibrate these instruments.

2. CATANIA ASTROPHYSICAL OBSERVATORY SPECTROPOLARIMETER

CAOS has been built to replace the old spectropolarimetric facility of the Catania Astrophysical Observatory (Leone et al. 2000; Leone & Catanzaro 2001). The main design requirements of CAOS were (Spanò et al. 2006) (1) linear and circular spectropolarimetry, (2) spectral resolution up to $R = 60{,}000$, (3) full spectral coverage in one exposure in the region: 388–725 nm, from calcium to lithium lines, and (4) fiber fed. Both integral light mode and polarimetric mode will feed two fibers for simultaneous measurements of source+sky or two independent polarimetric components, respectively.

2.1. Optical Design

In order to match the requirements, we designed a bench-mounted, fiber-fed, cross-dispersed échelle spectrograph. As a trade-off between resolution and cost, the spectrograph had a 10 cm collimated beam dispersed by a R4 échelle grating in white-pupil configuration (Dekker et al. 2000), with an optimized all-dioptric camera focusing the dispersed spectrum onto a CCD detector. Figure 2 shows the optical layout of the spectrograph as seen from the top.

2.2. Fiber Link and Pre-slit Optics

The CAOS spectrograph is fed with two 100 um, multimode, high-OH radicals, optical fibers that are optimized for UV transmission. One fiber is for the target and the other is for simultaneous calibration and/or sky substraction. At the Cassegrain focal plane, a couple of gradient-index lenses are glued on the input fiber ends projecting the pupil of the telescope on them. The lenses (by *Melles Griot*) have 1 mm focal distance, 1 mm diameter, a 0.37 numerical aperture and 0.25 fractional pitch. The fiber aperture projected on the sky is about 3″, with a typical 2″ seeing value at Mount Etna Observatory. The lenses convert the $F/15$ telescope beam into an $F/4$ beam into the fibers to reduce the so-called focal ratio degradation (Avila 1998). To convert the large $F/4$ exit optical aperture of the fibers into $F/10$ beams, two achromatic doublets and a single lens by *Optosigma* are used (Table 1). At the slit plane the two fibers appear with a diameter of 285 μm. The total efficiency of the fiber link, without considering seeing losses at the fiber input end is about 66%.

2.3. Collimator Mirrors

An $F/2.4$ paraboloidal mirror in Astrosital, with 400 mm clear area and a focal length of 1000 mm has been shaped and cut in two off-axis portions, as shown in Figure 3 by *Costruzioni Ottico Meccaniche Marcon*. Both portions have been coated with protected silver for high reflectivity (>97% at 0.5–1 μm) by *Gestione SILO*.

The larger portion has been used off-axis as an $F/10$ collimator. The mirror is used a second time creating an intermediate focal plane with light dispersed by the échelle grating. The second portion has been used to collimate the light toward the cross-disperser.

It is worth noting that the adopted solution is slightly different than classical white-pupil spectrographs, like UVES, SARG, or FEROS because there is no folding mirror at the return focus. This is to minimize the number of reflections, that is, to reduce the image quality degradation and light losses.

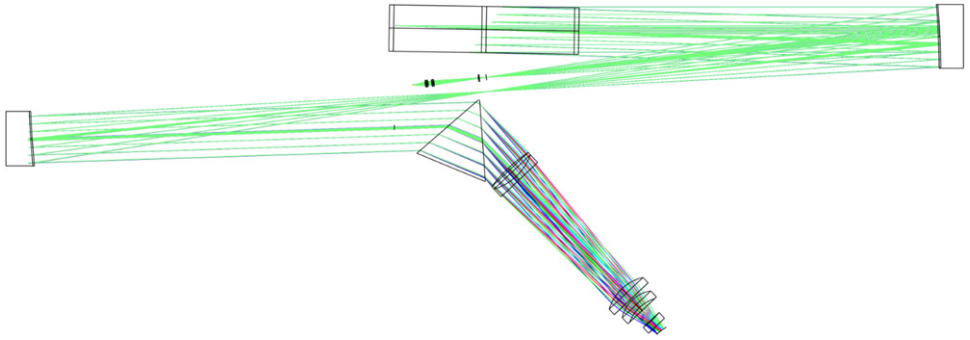

Figure 2. Optical layout of CAOS.

Table 1
Lens Prescription for the Pre-slit System. Distances are in Millimeters

Surface	Radius	Thickness	Material	Diam.
Fiber exit	⋯	28.263	⋯	⋯
First doublet	60.310	2.00	SF2	15
	17.600	4.90	BK7	15
	−23.395	7.426	Air	15
Second doublet	41.400	3.700	BK7	15
	−30.153	2.000	SF2	15
	−103.800	97.538	Air	15
Field lens	38.760	2.700	BK7	15
	∞	15.00	Air	15

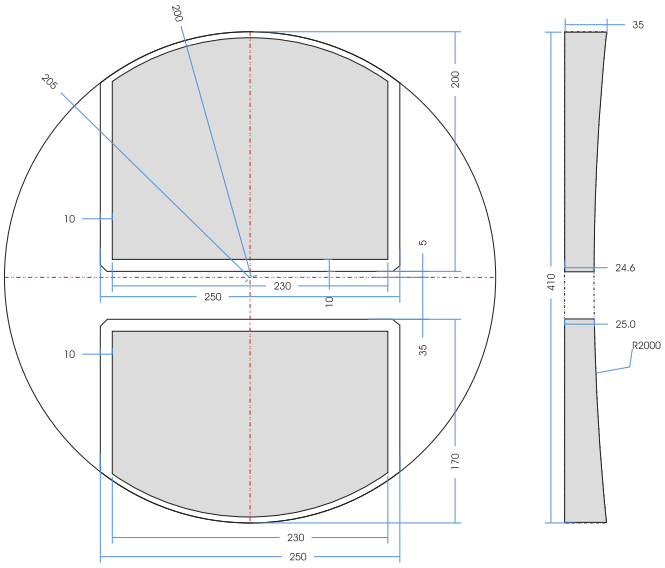

Figure 3. Collimators have been extruded from a 400 mm parabolic mirror. Measures are given in millimeters.

2.4. Grating

The échelle grating supplied by the *SPECTRA PHYSICS Richardson Gratings* presents 41, 59 rules mm^{-1} with a blaze angle of 76° (R4). The ruled area is 102 × 408 mm with an aluminum reflection coating. The grating works on the Littrow configuration with a small (0.°9) off-plane angle. Such a small angle introduces a small line tilt, below 0.2 pixel on the CCD (Section 2.7) focal plane.

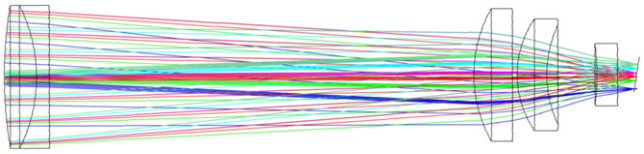

Figure 4. Camera layout. Spherical surfaces and standard glasses ensure high transmission and low cost. Note the tilted focal plane to correct for axial chromatism.

2.5. Cross-disperser

The *Gestione SILO* produced a 140 × 160 × 160 mm prism, made of Schott SF1, with an apex angle of 53.°1 that has been adopted as a cross-disperser. A/R coatings give an average throughput better than 90%. An analysis of the wavefront shows a deformation compatible with a degradation of the resolution equal to 8%. Degradation is ascribed to the non-homogeneous optical properties within the huge block of glass.

Fibers are rotated to have a projected distance with respect to the grating grooves equal to 570 μm. So that, when both fibers are illuminated, light overlapping is not present up to 856 nm.

2.6. Camera

The $F/2.1$ camera (Figure 4) was produced by *Société Européenne de Systèmes Optiques* and consists of five lenses mounted in three groups: a doublet, two separate lenses, and a field flattener acting also as a dewar window. All surfaces are spherical or plane.

Due to the fixed spectral format, axial chromatism has been corrected by tilting the focal plane. To assure the correct tilting of the focal plane, the last lens of the camera is also the window of the Dewar stopper and the detector is mounted on the tilted focal plane screwed on the internal side of the dewar flange at the focal distance.

The optical prescription for the camera is given in Table 2. First order parameters are as follows.

1. Entrance diameter: 100 mm.
2. Effective focal length: 213 mm.
3. F/number: $F/2.1$.
4. Field of view (diameter) : 7.°4.
5. Optimized wavelength range: 388–725 nm.

Table 2
Lens Prescription for the Camera (Distances Are in Millimeters)

Surface	Radius	Thickness	Material	Diam.
Object		∞		
Pupil		15.000		106
1	299.957	25.000	S-FPL51	112
2	−131.845	1.000		112
3	−130.009	10.000	S-BSL7	112
4	∞	344.586		112
5	91.285	30.000	S-BSL7	104
6	∞	1.000		104
7	64.249	23.000	S-BSL7	90
8	66.993	32.393		70
9	−194.150	8.000	S-BSL7	54
10	∞	15.000		54

2.7. Detector

The sensor used is an E2V42-40 Thinned and Back Illuminated High Performance Charge Coupled Device. It has a 2048 by 2048 pixel format, with 13.5 mm square pixels yielding an image area of 27.6 mm × 27.6 mm.

The CCD controller is a generation 3 CCD controller developed, built, and integrated on one of our cryostat at the Niels Bohr Institute in Copenhagen.

Reading the CCD at 100 kHz, the read-out noise is $3.5e^-$, $4e^-$ at 200 kHz and $6e^-$ at 400 kHz.

Table 3 shows the limits for any order of the echellogram imagined on the CCD. The resulting échelle spectral format covers the 376–1121 nm range in 81 orders, with only a 5% uncovered spectrum longword of 856 nm due to incomplete order overlapping.

2.8. Ghosts and Straylight

To locate ghosts in our echellogram, we have illuminated the fibers with a 633 nm laser light close to the CCD saturation. Figure 5 shows that there is not a ghost series in CAOS spectra due to periodic errors in grating rulings or any other feature at a level of 10^{-4} of the peak.

Light dispersed by the grating out of the collimator, scattering on non-ideal optical elements, and reflection on mechanical parts provide an origin for the stray light that hits the CCD irrespective of the diffraction law. Usually stray light is estimated by fitting the background signal present in the inter-order pixels and then subtracted it to the echellogram. In high-resolution spectroscopy, this is an important step in the data reduction procedure to obtain a spectrum with correct equivalent widths. As for CAOS, it results that stray light is less than 1% of the total light recorded by the CCD.

2.9. CAOS Stability

Spectrographs are limited in their accuracy by changes of the echellogram projection on CCD in time.

To handle the various sources of vibration noise (e.g., continuous Etna seismic activity, or building oscillation due to the Dome rotation), CAOS is mounted on a 2.4 × 1.2 m TMC optical table that provides dry dumping vibration cancellation.

Thermal variations change the optical path within a spectrograph resulting in transverse movements of the echellogram on the CCD and longitudinal variations responsible for the out of focus echellogram. Transverse variations are at the basis of errors in radial velocity measurements because

Table 3
For Any Order, the Minimum and Maximum Values of the Wavelengths in Nanometers

O	λ_i–λ_f	O	λ_i–λ_f	O	λ_i–λ_f	O	λ_i–λ_f
44	1103–1121	65	735–747	86	551–560	107	441–448
45	1077–1095	66	724–736	87	545–554	108	437–444
46	1053–1070	67	713–724	88	538–547	109	433–440
47	1029–1046	68	702–713	89	532–541	110	429–436
48	1007–1023	69	691–703	90	526–535	111	425–432
49	986–1002	70	681–692	91	520–529	112	421–428
50	965–981	71	671–682	92	515–523	113	417–424
51	945–961	72	662–673	93	509–517	114	413–420
52	926–942	73	652–663	94	503–512	115	410–417
53	908–923	74	643–654	95	498–506	116	406–413
54	891–905	75	634–645	96	493–501	117	402–409
55	874–888	76	626–636	97	487–496	118	399–406
56	858–872	77	618–628	98	482–490	119	396–402
57	842–856	78	609–619	99	477–485	120	392–399
58	827–841	79	601–611	100	472–480	121	389–396
59	813–826	80	594–604	101	468–476	122	386–392
60	799–812	81	586–596	102	463–471	123	382–389
61	785–798	82	579–588	103	458–466	124	379–386
62	772–785	83	572–581	104	454–462	125	376–383
63	759–772	84	565–574	105	449–457		
64	747–759	85	558–567	106	445–453		

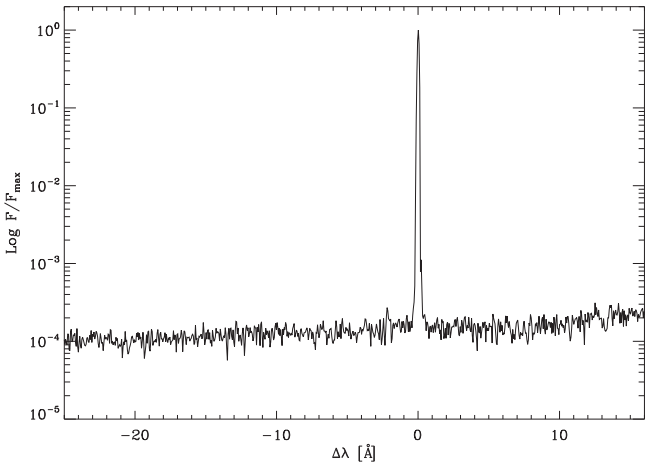

Figure 5. Observations of the laser line at 633 nm show no spurious lines due to imperfections in the gratings or other ghosts at a level of 10^{-4} of the peak.

the pixel-to-wavelength association is no longer correct. If the thermal variation temporal scale is longer than typical exposure times, then it is still possible to correct the wavelength scale. Historically, echellogram movements have been traced with an absorption cell, or simultaneously recording the echellogram of a calibration lamp. Often, telluric lines are used to set a zero point for wavelengths. Thermal variations shorter then exposure times result not only in a reduced wavelength calibration accuracy, but also in a decreased spectral resolution.

To reduce the effects due to thermal variations and improve the instrument stability as much as possible, CAOS is located in a thermally insulated room where temperature is kept constant within an rms <0.01 K.

As a test of stability during the instrument commissioning in 2014, we have obtained spectra of Vega with an S/N of ∼100. The barycenter of single spectral lines was found constant in time within an accuracy of ∼100 m s^{-1}. This value can be compared with the accuracy of HARPS-North, 60 m s^{-1} for an

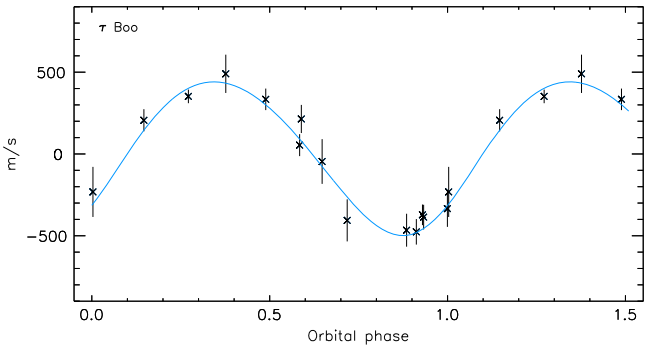

Figure 6. Simple correlation between chunks of CAOS (S/N ~ 50) spectra and a synthetic spectrum highlights the radial velocity variations of τ Boo. The continuum line has been drawn according the ephemeris listed by Drummond (2014).

S/N ~ 50, that has the same 0.01 K temperature stability but a double spectral resolution. During the commissioning, the well-known star τ Boo hosting an exo-planet has been monitored. A simple correlation between chunks of spectra at limited signal-to-noise (<50) and a synthetic spectrum[5] shows that radial velocities are accurate better than few hundred meters per second and in agreement with expectations (Figure 6). Velocities were analyzed using the *Image Reduction and Analysis Facility* (Tody 1986) packages; however, *ad hoc* algorithms are under development for an optimal measurement of radial velocities.

3. THE POLARIMETER

The CAOS polarimeter follows the design we adopted for the polarimetric unit of the high-resolution spectrograph (SARG) of the *Telescopio Nazionale Galileo* (Leone et al. 2003). The polarimeter is based on the double-beam technique and dual-waveplate method and it consists of a $\lambda/2$ or $\lambda/4$ retarder and a Savart plate working as a beam displacer. The polarimeter is located along the converging *F/15.5* beam of the telescope.

The polarizer is made from calcite, 15 × 15 mm^2 in size, with a total length of the two cemented parts of 32 mm, resulting in a beam separation of 2.5 mm in the visible range; both sides are AR coated for the 350–900 nm interval range. The Savart plate has been chosen because it gives null difference between the optical paths of the ordinary and extraordinary converging beams.

The retarders are achromatic ones. Because of the very large spectral interval covered by the CAOS in polarimetric mode (380–850 nm), low order or zero order retarders were not suitable, see Figure 2 in Leone et al. (2003). Super-achromatic retarders were discarded being sources of ripples already at resolutions of $R = 35{,}000$ (Donati et al. 1999). Unfortunately, the ideal Fresnel rhombs as $\lambda/2$ plate a K-prism as $\lambda/4$ plate are too big to be located along the telescope converging beams.

To align the fast axis of retarders with respect to the Savart plate acceptance axis, we have applied the Goodrich et al. (1995) method as described in Leone et al. (2003).

[5] The SYNTHE (Kurucz 2005) spectrum has been computed assuming the ATLAS9 (Kurucz 2005) model atmosphere with solar metallicity, $T_{\rm eff} = 3687$ K, and $\log g = 4.26$ (Valenti & Fischer 2005).

3.1. Observational Strategy and Data Reduction

The signal after the polarizer (Landi Degl'Innocenti & Landolfi 2004) is a function of the angle α between the retarder fast axis and polarizer acceptance axis, the angle β that the polarizer acceptance axis forms with the celestial meridian and the wave-plate retarder δ:

$$\begin{aligned} S(\alpha, \beta, \delta) \;=\; & 0.5\{I + (Q\cos 2\alpha + U\sin 2\alpha \\ & \times \cos[2(\beta-\alpha)] \\ & - (Q\sin 2\alpha - U\cos 2\alpha)\sin[2(\beta-\alpha)]\cos\delta \\ & + V\sin[2(\beta-\alpha)]\sin\delta\}. \end{aligned} \quad (1)$$

As usual, CAOS measures the Stokes parameters on the basis of a finite number of α values. Stokes V is measured with a quarter-wave-plate retarder ($\delta = \pi/2$) at $\alpha = +45°$ and $-45°$. By means of a half-wave-plate retarder ($\delta = \pi$), Stokes Q is measured with $\alpha = 0°$ and $45°$, while Stokes U for $\alpha = 22\overset{\circ}{.}5$ and $67\overset{\circ}{.}5$. To combine the *o*-rdinary and *e*-xtraordinary S beams emerging from the polarizer and measure the Stokes parameters, we follow the ratio method as introduced by Tinbergen & Rutten (1992). It is assumed that there is a time independent instrumental sensitivity $G(\lambda)$ (e.g., pixel-by-pixel efficiency) together with a time dependent sensitivity $F(\lambda)$ of spectra (e.g., variation of sky transparency). So that, a photon noise dominated Stokes parameter $P(\lambda)$ can be obtained from the recorded spectra at $\alpha = \alpha_1$ and α_2:

$$S_{\alpha_1,o}(\lambda) = 0.5\,[\,I(\lambda) + P(\lambda)]G_o(\lambda)F_{\alpha_1}(\lambda) \quad (2)$$

$$S_{\alpha_1,e}(\lambda) = 0.5\,[\,I(\lambda) - P(\lambda)]G_e(\lambda)F_{\alpha_1}(\lambda) \quad (3)$$

$$S_{\alpha_2,o}(\lambda) = 0.5\,[\,I(\lambda) - P(\lambda)]G_o(\lambda)F_{\alpha_2}(\lambda) \quad (4)$$

$$S_{\alpha_2,e}(\lambda) = 0.5\,[\,I(\lambda) + P(\lambda)]G_e(\lambda)F_{\alpha_2}(\lambda). \quad (5)$$

Hence,

$$\frac{P(\lambda)}{I(\lambda)} = \frac{R_P(\lambda)-1}{R_P(\lambda)+1} \quad \text{with} \quad R_P^2(\lambda) = \frac{S_{\alpha_1,o}(\lambda)/S_{\alpha_1,e}(\lambda)}{S_{\alpha_2,o}(\lambda)/S_{\alpha_2,e}(\lambda)}. \quad (6)$$

In addition, we compute the *Noise* polarization spectrum,

$$\frac{N(\lambda)}{I(\lambda)} = \frac{R_N(\lambda)-1}{R_N(\lambda)+1} \quad \text{with} \quad R_N^2(\lambda) = \frac{S_{\alpha_1,o}(\lambda)/S_{\alpha_2,e}(\lambda)}{S_{\alpha_2,o}(\lambda)/S_{\alpha_1,e}(\lambda)}, \quad (7)$$

to check for possible errors in Stokes $P(\lambda)/I(\lambda)$ due to the alignment of ordinary and extraordinary spectra in wavelength (Leone 2007). In such a context, it is worth pointing out the importance of the heliocentric velocity correction. For full Stokes polarimetry, a minimum of six exposures is necessary. Often a series of four exposures with a sequence α_1, α_2, α_2, α_1 is obtained to measure a Stokes parameter by subtracting any possible derivative in time. A 100 m s^{-1} radial velocity shift between the ordinary and extraordinary beams could let Stokes *V/I* be interpreted as a magnetic field of 100 Gauss (Leone & Catanzaro 2004). Unchecked alignements have been wrongly interpreted as the presence of magnetic fields on the central star of Planetary Nebulae (Leone et al. 2011).

CAOS Stokes profiles of γ Equ have been compared with similar spectra obtained with ESPADONS and HARPS-POL. Already reduced ESPADONS data have been obtained from the CFHT archive, whereas CAOS and HARPS-POL spectra

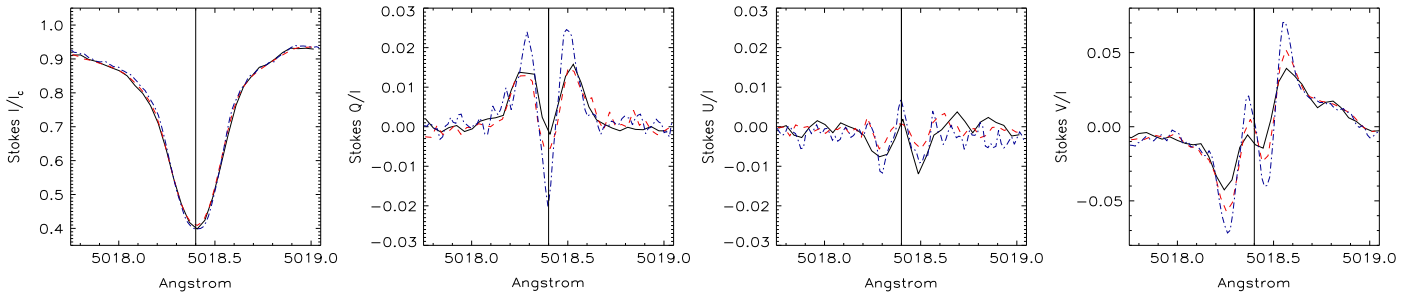

Figure 7. Stokes profiles of the γ Equ Fe I 5018.44 Å line as observed with CAOS (solid line), ESPADONS (red dashed line), and HARPS-POL (blue dotted–dashed line) are coincident within resolution and signal-to-noise.

have been extracted with the procedures previously described. Figure 7 shows that differences are within the spectral resolution and noise. This means that CAOS operativity and data reduction extraction procedures are within the present standard of worldwide polarimetric capabilities.

4. HIGH-RESOLUTION SPECTROPOLARIMETRY AND INSTRUMENTAL POLARIZATION

Generally speaking, there are three sources of instrumental polarization for a high-resolution spectropolarimeter.

(a) *Optics and mechanics* collecting photons and feeding the instrument. Polarization can be due to reflections and transmissions along the optical path before the polarimeter.

As to CAOS, no optics precedes the polarimeter and there are no opto-mechanical elements whose polarization changes continuously, like the tertiary mirror of an Alto-Azimuthal telescope (Giro et al. 2003). Indeed, there are no plane mirrors feeding the polarimeter and, because of the telescope axial symmetry, polarization is expected to be negligible. Sen & Kakati (1997) have shown that the polarization at an $f/13$ Cassegrain focus goes from 0.0018% to 0.016% for an unpolarized source observed in the range of 10–90 arcsec from the optical axis. Furthermore, they have shown that a 100% linear polarized source would be measured at a 99.998334% on axis up to 99.998184% if observed 90 arcsec off-axis.

(b) *Polarimeter components*, that in real life are far from being *ideal*.

Polarizers are characterized by an *extinction rate*, that is, the fraction of a fully polarized light traveling along the wrong path. Nominal extinction rate for the CAOS Savart plate is 10^{-5}. Whatever this extinction ratio with the wavelength is for CAOS, the swapping strategy of beam paths within the polarizer correct for.

Retarders present the nominal retardance only for a few wavelengths so that, at the other wavelengths, a fraction of a polarized state proceed along the "wrong" path of the polarizer. According to Bernhard Halle Nachfolger GmbH, CAOS retarders induce a retardance within $\pm 3\%$ of the nominal value in the 450–700 nm range with a correct value only at 488 and 633 nm. Bagnulo et al. (2009) have analytically shown that deviations from the nominal retardance are at the first order corrected by means of the beam-swapping technique. At high-resolution, retardance errors would then slightly modify the Zeeman shaped spectral lines. A result confirmed by numerical simulations of full Stokes polarimetry of the previously computed COSSAM Fe I 5018.44 Å line by applying Equations (1)–(6). Figure 8 shows the expected profiles for negative and positive differences on retardance. The expected Stokes Q, U, and V for a fully linear polarized radiation ($I = 1$, $Q = 1$, $U = 1$ and $V = 0$) because of a retardance error equal to -3% are $Q = 0.998$, $U = 0$, and $V = 0$, while a fully circular polarized radiation ($I = 1$, $Q = 0$, $U = 0$, and $V = 1$) would be observed as $Q = 0.047$, $U = 0.0$, and $V = 0.999$.

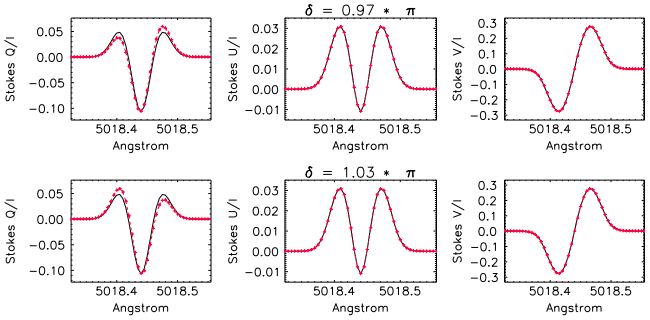

Figure 8. Cross-talk due to a $\pm 3\%$ deviation from the nominal retardance of wave plates can be quantified from line profiles shaped by the Zeeman effect. Intrinsic (solid) and expected (dashed) Stokes profiles of the Fe I 5018.44 Å line.

(c) *Fault of the assumption that the instrumental sensitivity is constant in time*. According to Equations (2)–(6), the *o*-rdinary and *e*-xtraordinary beams emerging from the polarizer should feed the spectrograph with an efficiency whose ratio $G_o(\lambda)/G_e(\lambda)$ is constant in time at any wavelength.

In standard spectroscopy, *Atmospheric Dispersion Correctors* or derotators, together with a telescope guiding system, are used to continuously feed slits or fibers with all wavelengths despite the terrestrial atmospheric refraction. Otherwise, certain wavelengths fall outside the slit or fibers and the resulting spectrum does not capture all of the light from the object. Thus only low-resolution spectroscopy can measure the absolute fluxes, by using slits much larger than the target image on the focal plane. At high resolution, when the slit is smaller than the target image, because of the combination of errors on autoguiding, the alignment with the parallactic angle, and the roughness of slit edges, only the flux relatively to the continuum can be accurately measured. Fiber injection errors are related to the optical apertures and alignments. In dual beam polarimetry, the combination of the Earth atmospheric refraction, always perpendicular to the horizon, and polarizer chromatism, differently affecting the ordinary and the extraordinary beams,[6] results in a rather complex chromatic

[6] In a simple Calcite or Foster prism (e.g., HARPS polarimeter), only the extraordinary beam is chromatically dispersed along the two beam direction. Chromatism in a Wollaston prism for both beams is along the separation direction. As for the two beams emerging from a Savart plate (e.g., ESPADONS or CAOS), the chromatism directions are mutually orthogonal and both are orthogonal to the conjunction of the two beams.

aberration that depends on the Earth atmosphere's temperature, pressure, and humidity as well as on telescope azimuth and altitude. As a consequence, the relative position of the two source images in monochromatic light changes, even continuously, on the telescope focal plane, where fibers are mechanically fixed, and it is difficult to get $G_o(\lambda)/G_e(\lambda)$ constant in time at the level that polarimetry requires. A further source of variability for the $G_o(\lambda)/G_e(\lambda)$ ratio is the temperature dependence of mechanics and optics, i.e., the gradient-index of lenses, distance of fibers, or coincidence of fiber and telescope axes. It is useful to remember that 1 arcsec is only 70μ on the CAOS fiber plane. The parameter N in Equation (7) can also measure the fault of this hypothesis in two exposures at times t_1 and t_2:

$$\frac{(G_o/G_e)_{t_1}}{(G_e/G_o)_{t_2}} = \frac{1+N}{1-N}. \quad (8)$$

Then, it appears that a fault of only 1% results in an instrumental polarization of 0.5%.

Cases (a) and (b) are handled by observing polarized standard stars. The same can also be seen if the G_o/G_e ratio depends on the α angle (Bagnulo et al. 2012), as expected for retarders whose two surfaces are not exactly parallel and/or whose rotation axes are not coincident with the telescope beam axis. Differently, the time variability of the instrumental sensitivity, case (c), cannot be modeled nor quantified on the basis of standard stars. It can only be evaluated a posteriori from the *Noise* spectrum on the basis of Equation (8), CAOS *Noise* spectra are usually null at 550 nm and increase up to 3% at the extreme wavelengths. Because of the previous variable chromatic aberation, the almost null instrumental polarization around 550 nm is probably a consequence of the telescope guiding system. This guarantees a better fiber injection for those wavelengths at which the guiding camera presents the largest sensitivity.

5. CALIBRATION

As stated before, photopolarimeters and low-resolution spectropolarimeters measure the absolute flux and are commonly limited to the linear polarization. Assuming that targets present no circular polarization, the instrumental polarization is determined on the basis of unpolarized and polarized standard stars. In the case of an astronomical source presenting linear and circular polarization, cross-talk from one polarization state to the other has to be evaluated.

To calibrate a high-resolution full Stokes spectropolarimeter, without reference to the polarized standard stars and including the possible conversion of a polarization state into the other, new methods have to be defined. Following Kuhn et al. (1994), that have modeled the instrumental polarization of the National Solar Observatory Vacuum Tower Telescope by observing the sunspot, we suggest calibrating high-resolution spectropolarimeters by observing the magnetic chemically peculiar (MCP) stars of the main sequence (Wolff 1983).

The relations between stellar magnetic fields and Stokes parameters have been given by Landi Degl'Innocenti & Landolfi (2004) for a weak line emerging from a surface element:

$$V(\lambda) = -4.67 \times 10^{-13} g \lambda^2 B_{||} \frac{\partial I}{\partial \lambda}$$
$$Q(\lambda) = -5.45 \times 10^{-26} G \lambda^4 B_{\perp} \cos 2\chi \frac{\partial^2 I}{\partial \lambda^2}$$
$$U(\lambda) = -5.45 \times 10^{-26} G \lambda^4 B_{\perp} \sin 2\chi \frac{\partial^2 I}{\partial \lambda^2}$$

with λ in angstroms, χ is the orientation angle of $B_\perp$ in a given reference system, g is the effective Landé factor, and G is the second-order effective Landé factor. Stokes parameters can be recovered by the observed ones via a Mueller matrix M, characterizing the instrumental polarization so that $[I, Q, U, V]_{\rm obs} = M_\lambda\, [I, Q, U, V]_{\rm inp}$. Since CAOS works at a Cassegrain focus, M_λ does not present variation with the telescope position. Following Kuhn et al. (1994), the inverse Mueller matrix is equal to

$$M_\lambda^{-1} = \begin{pmatrix} 1 & 0 & 0 & 0 \\ 0 & 1 + a_\lambda c_\lambda & a_\lambda d_\lambda & -a_\lambda \\ 0 & c_\lambda b_\lambda & 1 + d_\lambda b_\lambda & -b_\lambda \\ 0 & -c_\lambda & -d_\lambda & 1 \end{pmatrix}. \quad (9)$$

As a consequence of the large variety of Zeeman patterns (Stift & Leone 2003), very different Stokes profiles are observed in MCP stars. Figure 9 shows how different the Zeeman effect can be on three iron lines of the MCP star β CrB. Particularly important for our goals are lines, like the Fe II 6149.258 Å, with no linear polarization that immediately give the cross-talk from circular to linear polarization. While simple Zeeman triplets are expected to present no Stokes V signal at the central wavelength, and the measured signal is due to cross-talk from linear to circular polarization. To determine the coefficients of the Mueller matrix (9), we have carried out full Stokes spectropolarimetry of the very long period, $P > 70$ years (Leroy et al. 1994), MCP star γ Equ and of the MCP star β CrB along its 18.4868-day period (Bagnulo et al. 2001). γ Equ has been selected for the neglible rotational broadening, that allows Stokes V profiles to be very narrow, and Stokes Q and U profiles usually embedded in the noise. The few exceptions are lines with a very large second-order Landé factor, like the Fe I 5018.44 Å ($G = 3.67$, see Figure 10). On the other hand, β CrB presents well-defined Stokes Q and U, as well Stokes V profiles. The monitoring along the rotational period averages any possible wavelength shift of the zero value of Stokes V profiles.

We have determined the c_λ and d_λ coefficients of the CAOS inverse Mueller matrix assuming that the input Stokes Q and U line profiles presented by γ Equ are null. After correction for the cross-talk from Stokes V to Q and U in the spectropolarimetric data of β CrB, we determined the cross-talk from linear to circular polarization, that is a_λ and b_λ coefficients, assuming that that the observed $V_{\rm obs}$ profiles have to be null at the wavelengths of π components. It results that the coefficients of the Mueller matrix show a quadratic dependence on

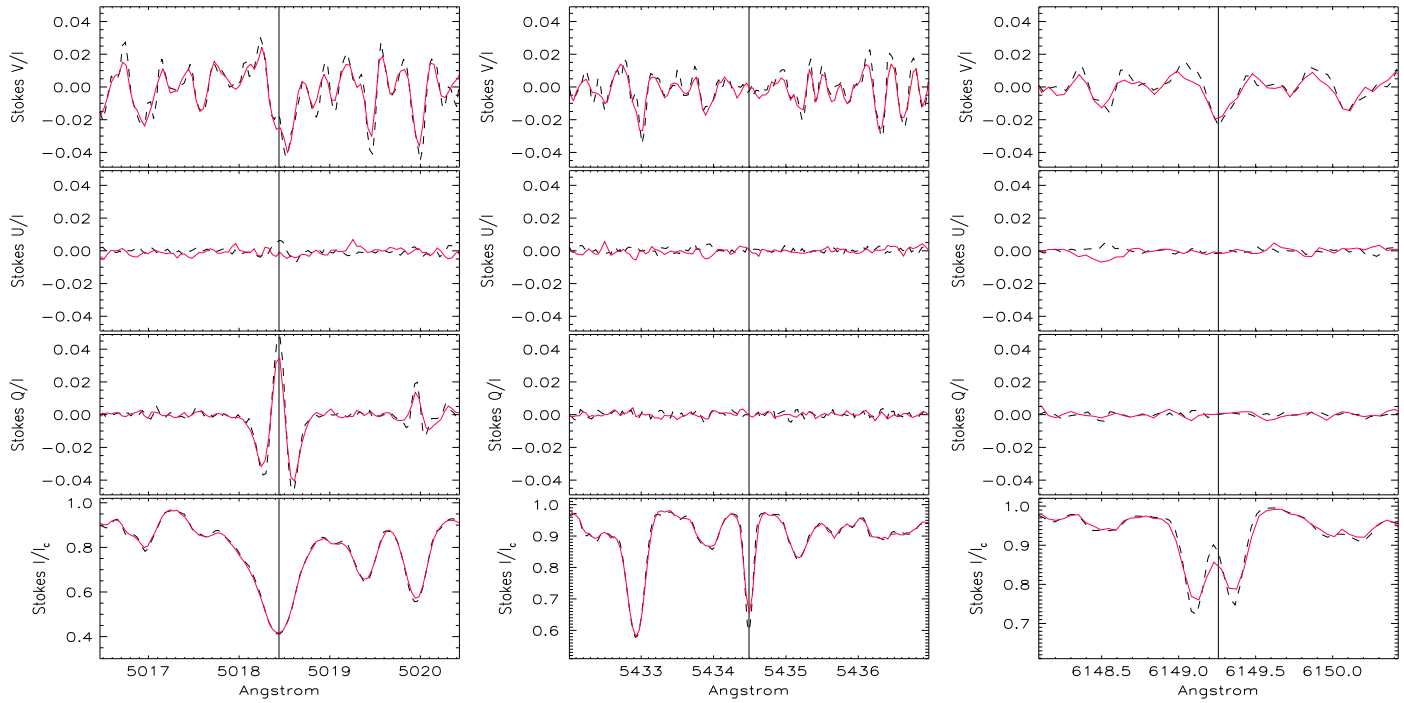

Figure 9. CAOS ($R = 55{,}000$, red solid line) observations of β CrB: (1) Fe II 6149.2λ line whose second-order effective Landé factor G is null and produces no linear polarization, (2) Fe I 5434.5λ line whose effective Landé factor is null and produces no circular polarization, and (3) Fe I 5018.4 Å line presenting one of the largest $G = 3.67$ values. For comparison ESPADONS ($R = 68{,}000$, dashed line) observations obtained at the same rotational phase ($\phi = 0.97$) are plotted.

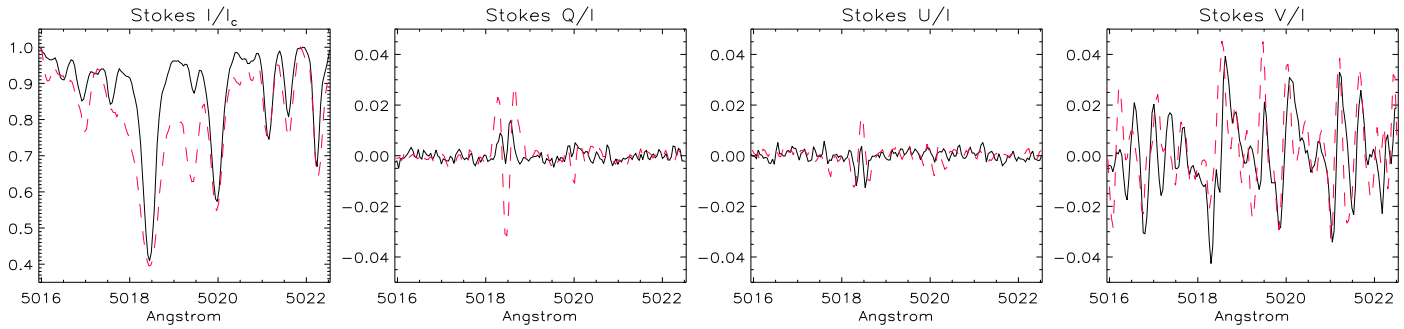

Figure 10. Stokes I, Q, U, and V profiles for γ Equ (solid line) and β CrB (dashed line).

wavelengths:

$$a_\lambda = -0.161 + 5.55 \times 10^{-5}\lambda - 4.60 \times 10^{-9}\lambda^2$$
$$b_\lambda = -0.131 + 4.80 \times 10^{-5}\lambda - 4.42 \times 10^{-9}\lambda^2$$
$$c_\lambda = +0.031 - 8.13 \times 10^{-6}\lambda + 5.04 \times 10^{-10}\lambda^2$$
$$d_\lambda = -0.370 + 1.33 \times 10^{-4}\lambda - 1.18 \times 10^{-8}\lambda^2.$$

It appears that CAOS cross-talk is almost negligible. A maximum of 0.4% of Stokes Q and U is converted in V. While the upper-limit of cross-talk from V to U is 2.7% at 400 nm. The quadratic dependence of inverse matrix coefficients on the wavelength closely resembles the behavior of the retardance of achromatic retarders (Leone et al. 2003) and it suggests that most of cross-talk is due to the incorrect retardance of wave plates. According to the Bernhard Halle Nachfolger GmbH, CAOS retarders induce a retardance within $\pm 3\%$ of the nominal value in the 450–700 nm range with a correct value only at 488 and 633 nm. It is worth noting that $d_{488\,\mathrm{nm}} = -0.20\%$ and $d_{633\,\mathrm{nm}} = -0.09\%$.

6. SUMMARY

We have presented the new CAOS based on a fiber-fed white-pupil spectrograph able to perform full Stokes polarimetry. The $\tan\theta = 4.0$ échelle grating and a glass prism cross-disperser record in a single exposure wavelength from 375 to 1100 nm with a resolution of up to $R = 55{,}000$. Small uncovered spectral regions are longward to 856 nm.

Linked at the 36-inch telescope with fibers whose FoV is 3 arcsec, CAOS is able to achieve, at $R = 55{,}000$, an S/N = 60 for a $V = 10$ star in one hour. About 30% of the light has been estimated to be lost because of the telescope guiding system. A new telescope interface with a tip-tilting mirror for guiding is under development.

Thermalized with an rms smaller than 0.01 K, CAOS echellogram is stable to guarantee radial velocity measurements better than 100 m s^{-1} from a single spectral line of Vega acquired with an S/N = 100.

With the exception of the achromatic retarders, the CAOS polarimeter is a copy of the polarimetric unit of SARG, the former high-resolution spectrograph of the Telescopio

Nazionale Galileo. CAOS Stokes spectral line profiles are consistent within errors with the results of similar instruments, like ESPADONS and HARPS-south.

As is expected for any high-resolution spectrograph, CAOS cannot measure absolute fluxes and, as a consequence, unpolarized and polarized standard stars cannot be used to determine the instrumental polarization. Measurements of unpolarized standard stars can present a signal up to 3%. After subtracting the spurious continuum polarization, a method has been implemented to measure the cross-talk on the basis of spectral lines formed in the presence of magnetic fields. Observations of the chemically peculiar stars β CrB and γ Equ show that the cross-talk can be entirely ascribed to the incorrect retardance of wave plates and, as analytically stated by Bagnulo et al. (2009), it can be almost negligible by adopting the beam-swapping technique. A result that confirms the negligible instrumental polarization in the focal plane of Cassegrain telescopes (Sen & Kakati 1997) in the absence of tilted mirrors feeding a polarimeter.

We thank Dr. Andersen and Dr. Preben for their help with the CCD controller.

REFERENCES

Avila, G. 1998, ASPC, 152, 329
Bagnulo, S., Fossati, L., Kochukhov, O., & Landstreet, J. D. 2013, A&A, 559, 103
Bagnulo, S., Landolfi, M., Landstreet, J. D., et al. 2009, PASP, 121, 993
Bagnulo, S., Landstreet, J. D., Fossati, L., & Kochukhov, O. 2012, A&A, 538, 129
Bagnulo, S., Wade, G. A., Donati, J.-F., et al. 2001, A&A, 369, 881
Clarke, D., & Naghizadeh-Khouei, J. 2000, P&SS, 48, 285
Covino, S., Molinari, E., Bruno, P., et al. 2014, AN, 335, 117
Dekker, H., D'Odorico, S., Kaufer, A., Delabre, B., & Kotzlowski, H. 2000, Proc. SPIE, 4008, 534
Donati, J.-F., Catala, C., Wade, G. A., et al. 1999, A&AS, 134, 149
Drummond, J. D. 2014, AJ, 147, 65
Giro, E., Bonoli, C., Leone, F., et al. 2003, Proc. SPIE, 4843, 456
Goodrich, R. W., Cohen, M. H., & Putney, A. 1995, PASP, 107, 179
Harrington, D. M., Kuhn, J. R., & Hall, S. 2011, PASP, 123, 799
Kuhn, J. R., Balasubramaniam, K. S., Kopp, G., & Penn, M. J. 1994, SoPh, 153, 143
Kurucz, R. L. 2005, MSAIS, 8, 14
Landi Degl'Innocenti, E., & Landolfi, M. 2004, in Astrophysics and Space Science Library, Polarization in Spectral Lines (Vol. 307; Dordrecht: Kluwer)
Leone, F. 2007, MNRAS, 382, 1690
Leone, F., Bruno, P., Calì, A., et al. 2003, Proc. SPIE, 4843, 465
Leone, F., Catalano, S., & Catanzaro, G. 2000, A&A, 355, 315
Leone, F., & Catanzaro, G. 2001, A&A, 365, 118
Leone, F., & Catanzaro, G. 2004, A&A, 425, 271
Leone, F., Cecconi, M., Cosentino, R., et al. 2014, Proc. SPIE, 9147, 91472
Leone, F., Martínez González, M. J., Corradi, R. L. M., Privitera, G., & Manso Sainz, R. 2011, ApJL, 731, 33
Leroy, J. L., Bagnulo, S., Landolfi, M., & Landi Degl'Innocenti, E. 1994, A&A, 284, 174
Sen, A. K., & Kakati, M. 1997, A&AS, 126, 113
Serkowski, K. 1974, in Polarization Techniques (New York: Academic Press), 361
Solanki, S. K., & Stenflo, J. O. 1986, A&A, 170, 120
Spanò, P., Leone, F., Bruno, P., et al. 2006, MSAIS, 9, 481
Sterzik, M. F., Bagnulo, S., & Palle, E. 2012, Natur, 483, 64
Stift, M. J., & Leone, F. 2003, A&A, 398, 411
Stift, M. J., Leone, F., & Cowley, C. R. 2012, MNRAS, 419, 2912
Strassmeier, K., Ilyin, I., Järvinen, A., et al. 2015, AN, 336, 324
Tinbergen, J., & Rutten, R. 1992, A User's Guide to WHT Spectropolarimetry (ING; La Palma User Manual No. 21)
Tody, D. 1986, Proc. SPIE, 627, 733
Trujillo-Bueno, J., Moreno-Insertis, F., & Sanchez Martinez, F. 2002, in Proc. of the XII Canary Islands Winter School of Astrophysics, Astrophysical spectropolarimetry, ed. J. Trujillo-Bueno, F. Moreno-Insertis, & F. Sánchez (Cambridge: Cambridge Univ. Press)
Valenti, J. A., & Fischer, D. A. 2005, ApJ, 159, 141
Wolff, S. C. 1983, A-Stars: Problems and Perspectives (NASA SP-46; Washington, D.C.: NASA), 33